JOURNAL OF CATALYSIS 56, 407–429 (1979)

Catalytic Synthesis of Methanol from CO/H_2

I. Phase Composition, Electronic Properties, and Activities of the $Cu/ZnO/M_2O_3$ Catalysts

R. G. HERMAN, K. KLIER, G. W. SIMMONS, B. P. FINN, AND J. B. BULKO

Center for Surface and Coatings Research, Lehigh University, Bethlehem, Pennsylvania 18015

AND

T. P. KOBYLINSKI

Process Research Division, Gulf Research and Development Company, P. O. Drawer 2038, Pittsburgh, Pennsylvania 15230

Received August 16, 1978

The low pressure methanol synthesis catalysts Cu/ZnO, $Cu/ZnO/Al_2O_3$, and $Cu/ZnO/Cr_2O_3$ were found to contain a new compound identified as a Cu^I solution in ZnO, which is also an active component of the above catalysts. Combined X-ray diffraction, optical, and XPS–Auger studies are presented that describe the formation, electronic structure, and surface composition of these catalysts. In particular, the surface of the working catalyst is free of carbon, both in the presence and absence of CO_2 in the feed gas. A synthesis mechanism is proposed whereby the Cu^I centers nondissociatively chemisorb and activate carbon monoxide and the ZnO surface activates hydrogen. Catalyst deactivation in CO/H_2 mixture is explained as the reduction of Cu^I to inactive copper metal, while the rate enhancing effect of O_2, H_2O, and CO_2 is due to the maintenance of an oxidation potential high enough to keep the copper in the active Cu^I state. No special pore distribution or presence of crystalline phases such as spinels is necessary for selectivity of the Cu/ZnO catalyst to the formation of methanol.

INTRODUCTION

Among the many processes for making oxygenated products from carbon monoxide and hydrogen, the catalytic synthesis of methanol stands out with its high selectivity, long term performance of the catalysts, and lack of catalyst poisoning by oxidizing gases. The industrial low pressure (20–100 atm) catalysts are invariably based on the compositions $Cu/ZnO/Cr_2O_3$ or $Cu/ZnO/Al_2O_3$. Tables 1 and 2 show the reaction conditions and compositional variations in the various patent claims as well as in some open literature. An interesting feature of these catalysts, and one encountered less frequently than is commonly believed, is the fact that the mixed catalysts are at least three orders of magnitude more active than each of the separate catalyst components. The disadvantages of the $Cu/ZnO/Al_2O_3$ or Cr_2O_3 catalysts are few but significant: low resistance to thermal shocks, which does not allow the catalyst to be operated above 300°C, and extreme sensitivity to sulfur and chlorine poisoning (*16*) that requires a careful and expensive purification of the synthesis gas.

0021-9517/79/030407-23$02.00/0

TABLE 1

Cu–Zn–Al Oxide Catalysts Used in the Synthesis of Methanol

Composition[a] (wt%)	Reactants[b]	Temp. (°C)	Pressure (atm)	Space velocity (hr^{-1})	Yield (kg/liter/hr)	Company	Reference
12:62:25	2	230	200	10,000	3.290	BASF	1
	2	230	100	10,000	2.086	BASF	
23:46:30	3	240		20,000	2.5	CCI	2
24:38:38	2	226	50	12,000	0.7	ICI	3
35:45:20	1	250				Academic	4
53:27:6	1	250	50			ICI	5
60:22:8	1	250	50	40,000	0.5	ICI	6
	2	226	100	9,600	0.5	ICI	
64:32:4	3	250	50	10,000	0.3	Academic	7
	3	300	50	10,000	0.9	Academic	
66:17:17	1	275	70	200[d]	4.75	DuPont	8
[c]	1	250	50	10,000		Academic	9

[a] $CuO:ZnO:Al_2O_3$.
[b] 1 = $H_2 + CO + CO_2$, 2 = $H_2 + CO + CO_2 + CH_4$, 3 = $CO + H_2$, N_2 is sometimes used as a diluent.
[c] SNM-1 catalyst.
[d] Moles per hour.

In the commercial production of methanol, it has been found desirable for the synthesis gas to contain a certain amount of carbon dioxide, e.g., approximately 6 vol% (*14*, *17*). During the methanol synthesis reaction, the CO_2 could function in a number of capacities; it could (a) oxidize the catalyst and maintain it in an active

TABLE 2

Cu–Zn–Cr Oxide Catalysts Used in the Synthesis of Methanol

Composition[a] (wt%)	Reactants[b]	Temp. (°C)	Pressure (atm)	Space velocity (hr^{-1})	Yield (kg/liter/hr)	Company	Reference
11:70:19	3	250		4,000		Power–Gas Corp.	10
15:48:37	3	270	145	10,000	1.95[c]	Jap. Gas–Chem. Co.	11
31:38:5	3	230	50	10,000	0.755	BASF	12
	4	230	50	10,000	1.275	BASF	
33:31:36	3	250	150	10,000	1.1	Academic	7
	3	300	150	10,000	2.2	Academic	
40:10:50	1	260	100	10,000	0.48[c]	T, HFA	13
40:40:20	2	250	40	6,000	0.26	ICI	14
	2	250	80	10,000	0.77	ICI	
60:30:10	1	250	100	9,800	2.28	Metall-Gesellschaft	15

[a] $CuO:ZnO:Cr_2O_3$.
[b] 1 = $H_2 + CO + CO_2$, 2 = $H_2 + CO + CO_2 + CH_4$, 3 = $CO + H_2$, 4 = $CO + H_2 + O_2$, N_2 is sometimes used a a diluent.
[c] Kilograms per kilogram per hour.

state, (b) be converted directly to methanol, or (c) prevent carbon fouling of the catalyst by oxidizing surface carbon species. While in earlier kinetic investigations (*17*, *18*) the role of carbon dioxide was passed unnoticed, the authors of the more recent studies (*19–22*) proposed that CO_2 is directly, and more rapidly than CO, hydrogenated to methanol. In contradiction with the latter proposition is the fact that conditions can be found under which CO_2 is not consumed in methanol synthesis from $H_2/CO/CO_2$ mixtures and that the shift reaction between carbon monoxide and water to produce CO_2 and hydrogen does not proceed substantially faster than methanol synthesis (*20*), as would be required if CO_2 were hydrogenated to methanol and then regenerated by the shift reaction. The promotion effect of CO_2 is definite, however, and quite unique to the $Cu/ZnO/Al_2O_3$ or $Cu/ZnO/Cr_2O_3$ catalysts. On other recently reported low pressure catalysts, such as Pd/SiO_2, Pt/SiO_2, and Ir/SiO_2 (*23*), the methanol synthesis was inhibited by the presence of CO_2 in the syngas.

The question of the effect of CO_2 on the synthesis over the copper-based catalysts is associated with an even more fundamental question concerning the nature and origin of the mutual promotion of the copper, zinc oxide, and a support to form a catalyst that is orders of magnitude more active and substantially more selective than its individual components. In a recent investigation of a number of $Cu/ZnO/Al_2O_3$ catalysts, Shimomura *et al.* (*24*) established that the variations of catalytic activity in these systems closely followed the variations of the extent of carbon monoxide chemisorption and that the highest activity required the catalyst components to coexist in a fine interdispersion. The present investigation aims at determining the nature of interactions that give rise to the active sites enhancing the catalyst activity and carbon monoxide chemisorption. Since the interactions among the catalyst components occur on a scale involving microscopic distances in highly dispersed media, it appeared necessary to carry out a detailed characterization of a number of catalyst compositions by X-ray diffraction, optical, Auger and X-ray photoelectron spectroscopies, BET-pore distribution measurements, and microdiffraction–microanalysis studies in the electron microscope. This communication reports on the phase composition during all stages of catalyst preparation and use, the identification and electronic properties of a Cu/ZnO solution that was found to be present in the active phase, and the pore structure of laboratory prepared as well as of commercial catalysts. A model was established that satisfactorily accounts for the mutual promotion of the catalyst components as well as for the effects, both rate enhancing and retarding, of various gas admixtures and impurities. Studies of catalyst morphology, single particle structure and orientation, and elemental composition of single crystallites, which further reinforce the proposed model, are reported in a subsequent communication (*25*).

EXPERIMENTAL

Testing apparatus. The catalyst activity was evaluated in a pressure unit (Fig. 1) equipped with a flow reactor and with pressure, flow rate, and temperature controls. The catalytic reactor consisted of 1.27-cm i.d., 316 stainless steel tubing fitted with a 0.32-cm o.d. thermowell and a volume permitting testing of catalyst samples ranging in size from 1.0 to 35 cm^3. Testing at pressures up to and including 100 atm (1 atm = 101.3 kN/m^2) could be carried out.

Downstream from the reactor, the pressure was reduced to atmospheric by a pressure-pilot-controlled Research valve, and the product mixture was led through a heated stainless steel tube to the gas sampling valve of a gas chromatograph.

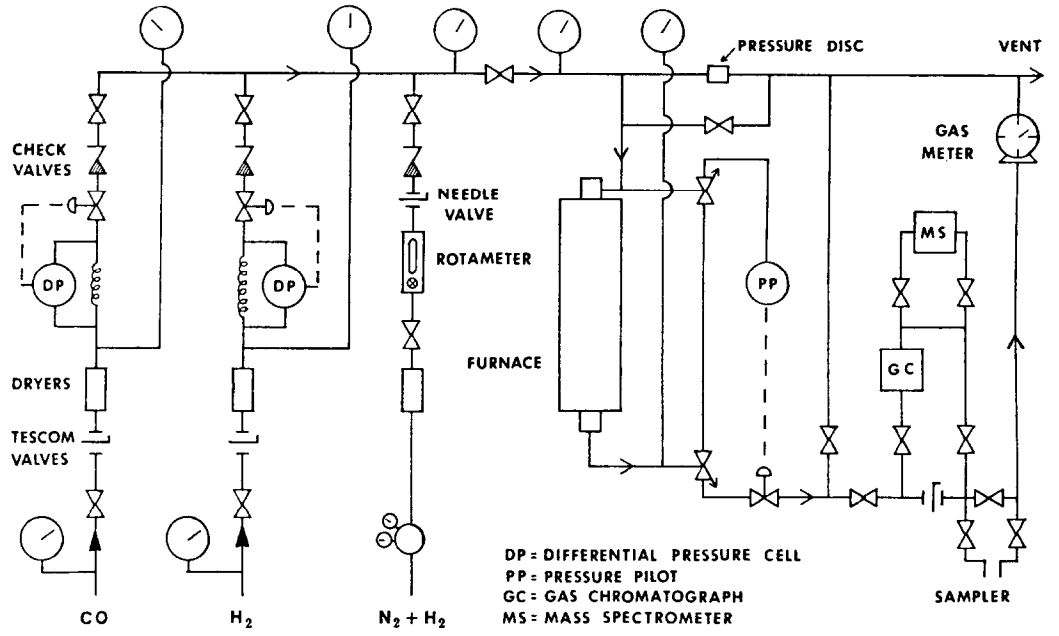

FIG. 1. A diagram of the low pressure reactor system used to test methanol synthesis catalysts.

The HP 5730A model coupled with a HP 3380A reporting integrator was used for quantitative analysis of the products. All gases in this work were high purity (CO, CO_2, and $O_2 > 99.3\%$; $H_2 > 99.995\%$) and were obtained, either pure or premixed to desired compositions, from Air Products and Chemicals.

Catalyst preparation. Catalysts were prepared so as to vary the chemical composition from pure components to ternary mixtures in order to identify the compound active in the low pressure methanol synthesis. A series of copper–zinc oxide catalysts with final composition ranging from pure zinc oxide to pure copper was prepared by coprecipitation of basic salts of copper and zinc from approximately 1 *M* nitrate solutions by dropwise addition of 1 *M* sodium carbonate at 85 to 90°C until the pH was raised from approximately 3 to between 6.8 and 7.0. The reaction typically took 1.5 hr and consumed between 350 and 450 ml of the Na_2CO_3 solution per 1500 ml of the (Cu, Zn) nitrate solution. Following a 1.5 hr digestion while the solution cooled, the precipitate was collected on a fritted glass filter and was washed thoroughly with distilled water. The samples were then dried overnight at 60 to 110°C. The subsequent calcination was carried out in air by heating the catalyst sample in a furnace from 150 to 350°C in increments of 50°C every 30 min with the maximum temperature maintained for 3 hr. X-ray analysis showed that a mixture of CuO (*26*) and ZnO (*27*) was obtained after the calcination. The oxides were pelletized from aqueous slurries, dried at ambient temperature, and then broken to a uniform 10 to 20 mesh size. The catalyst samples (typically 3 ml) were placed in the reactor (Fig. 1) and reduced in 2% H_2 in N_2 (1 atm) at 250°C at a flow rate of approximately 4 liters/hr for 4 to 20 hr. Samples for X-ray diffraction, surface area measurements, Auger spectroscopic and optical measurements were taken before and after the catalyst use and maintained in an N_2 atmosphere to avoid reoxidation.

The Cu/Zn/Al and Cu/Zn/Cr catalysts

were prepared and treated using the same techniques and procedures as described for the binary system. The third component was added by coprecipitation of the catalyst precursors from nitrate solution or by the direct addition of the oxide (Al_2O_3 or Cr_2O_3) to the hot solution prior to or subsequent to the coprecipitation of the copper and zinc components. One Cu/Zn/Al catalyst was synthesized by coprecipitation from acetate solution.

X-ray powder diffraction. The powder patterns were obtained by using a Siemens X-ray diffractometer with CuK_α radiation. Samples were briefly exposed to air, mounted on a glass slide using double-seal tape and inserted into the sample holder. Values for *d*-spacings listed in Ref. (*28*) were used to identify the compounds contributing to the diffraction pattern. After a compound has been identified, its diffraction pattern was computed from a published structure, using the tabulated atomic scattering factors (*29*) and making corrections for multiplicity of reflections, geometrical and polarization factors according to Eq. (1)

$$I = NK\frac{1}{V^2}|F|^2 p\left[\frac{1+\cos^2 2\theta}{\sin^2\theta\cos\theta}\right], \quad (1)$$

where I is the intensity of an X-ray diffraction line, N is the number of unit cells in the irradiated volume, K is a constant common to all structures, V is the volume of the unit cell, $|F|^2$ is the complex square of the structure factor, p is the multiplicity of the reflection, and the last term is the Lorentz polarization factor (*30*). The structure factors of the reflections of each of the investigated compounds were calculated from the tabulated atomic scattering factors. No corrections were made or deemed necessary for absorption of CuK_α radiation in the samples. A comparison of experimental intensities with the calculated ones for all pure compounds investigated here showed an agreement satisfactory for using the X-ray intensities for a quantitative analysis of mixtures. This analysis naturally excludes any morphous compounds but does account for line broadening due to microcrystallinity by taking areas under the diffraction peaks rather than peak heights as a measure of diffraction intensities.

Auger and X-ray photoelectron spectroscopic analyses. The Auger analyses were carried out in the Physical Electronics Auger Spectrometer (Phi Model 50-220) equipped with a cylindrical mirror analyzer. The catalyst samples were exposed to air, pressed into an indium foil and inserted into the sample holder. Following evacuation, the analyses were carried out with particular attention to Cu, Zn, O, Cr, Al, C, S, Cl, Na, and Ca. No traces of Cl, Na, or Ca were found in any of the samples investigated here. (Some samples were depth-profiled by ion sputtering in the Auger spectrometer.) The X-ray photoelectron (XPS) analyses were performed using the Physical Electronics ESCA–Auger Spectrometer Model 548. The sample preparation was the same as in the previous case.

Optical spectroscopy. Optical measurements were carried out by utilizing a Cary 14R spectrometer in the range of wavelengths from 200 to 2400 nm, covering the uv, visible, and near-infrared regions. The samples were placed in infrasil front window cells (*31*) without exposure to air, either by transfer under nitrogen or by a direct reduction in a closed system containing the optical cell by a procedure identical to that described in the Catalyst Preparation section. MgO standards were employed, and the optical data were represented as $F(R_\infty) = (1 - R_\infty)^2/(2R_\infty)$, where R_∞ is the reflectance from a semi-infinite sample relative to the standard (*31*).

Surface areas and pore distribution determinations. A standard BET method was used for the determination of surface areas from argon adsorption at −195°C. An

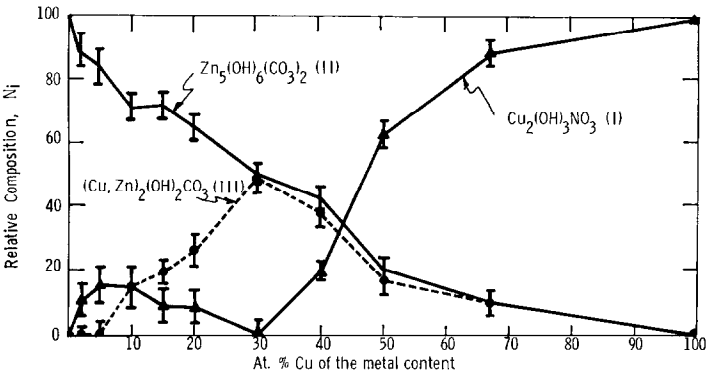

FIG. 2. The compositional profile of the Cu/Zn system determined by X-ray powder diffraction of the catalyst precursors formed from nitrate solution by carbonate precipitation.

argon area of 0.168 nm^2 was used in the calculations of monolayer areas.

The mesopore distribution was determined by analysis of the adsorption–desorption isotherms based on Brunauer's corrected modelless method and its analytical modification (*32*, *33*), and the micropore volume was calculated according to Sing (*34*).

RESULTS

Phase Composition of the Catalyst Precursors and of the Catalysts

The Cu–Zn precipitates. The X-ray powder patterns of the precipitates from Cu–Zn nitrate solutions showed the presence of three compounds, $Cu_2(OH)_3NO_3$(I), $Zn_5(OH)_6(CO_3)_2$(II), and $(Cu, Zn)_2(OH)_2CO_3$(III). The relative proportions of these compounds were determined by the initial Cu:Zn ratio in the solution. The diffraction patterns of compounds I, II, and III accounted for all the lines in each of the mixed precipitates. Figure 2 shows the relative abundances N_i of compounds I, II, and III, calculated from the observed diffraction intensities I_i according to Eq. (1) in which the structure factor was determined from the published structures of compounds I (*35*), II (*36*), and III (*37*) and the atomic scattering factors were taken from tables as outlined in the Experimental section. The structure used for Compound III was actually that of malachite, $Cu_2(OH)_2CO_3$ (*37*), with which Compound III is isomorphous.

Calcined CuO ZnO samples. After the

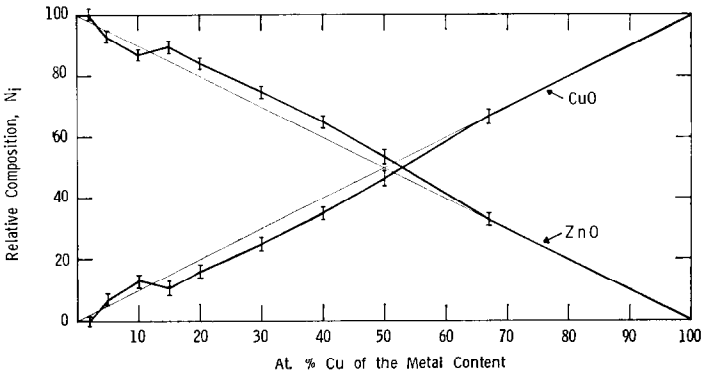

FIG. 3. The compositional profile determined by X-ray powder diffraction following calcination of the Cu/Zn precursor samples to 350°C.

final calcination step at 350°C (3 hr), all mixed precipitates of compounds I, II, and III formed a two-phase system consisting of hexagonal ZnO (*27*) and tetragonal CuO (*26*) of relative abundances as shown in Fig. 3. Beginning with 15% CuO/85% ZnO, the samples showed 2 to 4% less than the theoretical amount of CuO. This result suggests that 2 to 4% of CuO is dissolved in ZnO. Further evidence of solution of Cu in ZnO has been obtained from electron-induced X-ray fluorescence analysis in the scanning transmission electron microscope (*25*). Although the concentrations of the crystalline phases of CuO and ZnO vary uniformly throughout the whole compositional range, there are two ranges of ZnO morphologies, one between 0 and 30% CuO, in which the ZnO appears in the form of a network of crystallites with their sixfold crystal axis parallel to the major dimension, and another between 40 and 80% CuO, in which the ZnO crystallites are hexagonal platelets with the sixfold crystal axis perpendicular to the major dimensions (*25*).

Reduced and used Cu–ZnO catalysts. Upon reduction at conditions specified in the Experimental section, the product consisted of metallic copper and hexagonal ZnO. Electron microscopic investigations showed that the ZnO particles did not change their crystal habit described in the previous paragraph while the copper assumed spherical (for 10–40% CuO samples) or irregular blunted (for 50–67% CuO samples) shapes (*25*). Neither the phase composition nor crystallite morphology of the reduced catalysts changed upon a regular use in methanol synthesis under the conditions reported in this work.

The $Cu/ZnO/Cr_2O_3$ and $Cu/ZnO/Al_2O_3$ catalysts. There are numerous ways to prepare the $Cu/ZnO/Al_2O_3$ or $Cu/ZnO/Cr_2O_3$ catalysts, and many of the published preparations were examined in our characterization studies. Only an outline of the results pertinent to discussion of the support effects will be given here. In most cases, the phase compositions of the ternary catalysts after calcination and reduction were the same as in the Cu/ZnO system with additional lines of crystalline Al_2O_3 or Cr_2O_3, as illustrated in Fig. 4. In some preparations involving alumina, very high dispersion and considerable amounts of amorphous phases were indicated by X-ray diffraction line broadening or even by the absence of certain or all reflections. It should be noted that spinels were previously identified in the alumina-based catalysts and suggested to be the carriers of catalytic activity (*38*); however, no evidence for spinels was obtained in the present work. The morphologies of the copper and zinc oxide components in the alumina or chromia containing catalysts were similar to those in the alumina or chromia free copper–zinc oxide system.

Surface Composition of the Catalyst Precursors and of the Catalysts

Surface analysis of selected catalyst precursors, reduced catalysts, and used catalysts was carried out by X-ray photoelectron and Auger spectroscopies. The precipitate precursors containing 5, 30, and 67% Cu were subject to XPS/Auger analysis that showed all the expected elemental constituents and no impurities such as S, Cl, Na, and Ca. More detailed analysis of the 67% Cu precursor provided evidence of two superimposed oxygen 1*s* peaks, a major one at 535 eV and a minor one at 529 eV. A significant carbon 1*s* but only a very small nitrogen 1*s* peak was observed despite the large quantity of nitrate in the sample, indicating that the nitrate groups were not on the surface; in view of this observation, the 535 eV oxygen peak is assigned to hydroxyl and the small shoulder at 529 eV to carbonate oxygen. This assignment is based upon the relative abundances of copper hydroxynitrate and copper

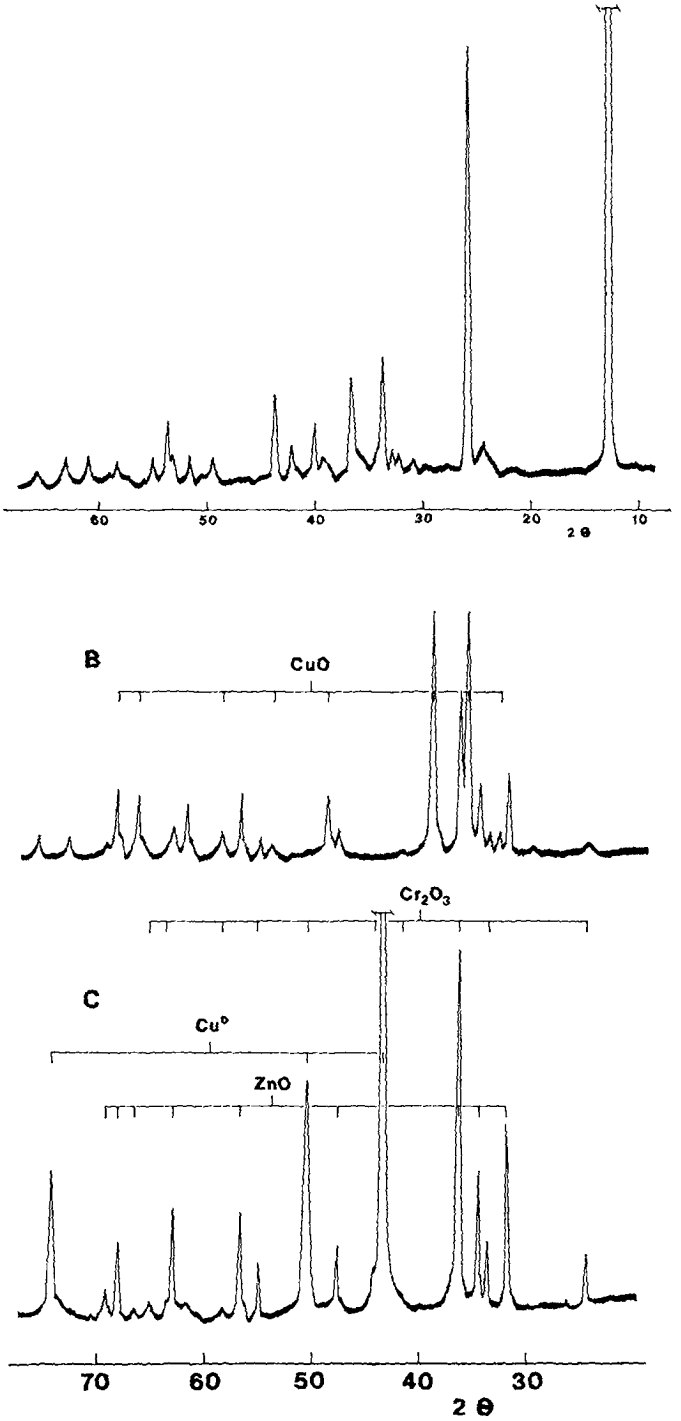

FIG. 4. The X-ray powder diffraction patterns of the Cu/Zn/Cr (60:30:10) catalyst (A) after precipitation and drying, (B) after calcination at 350°C, and (C) after reduction at 250°C by a 2% H_2/98% N_2 mixture. Pattern A corresponds mainly to $Cu_2(OH)_3NO_3$, and the unassigned lines in pattern B are due to ZnO and to Cr_2O_3.

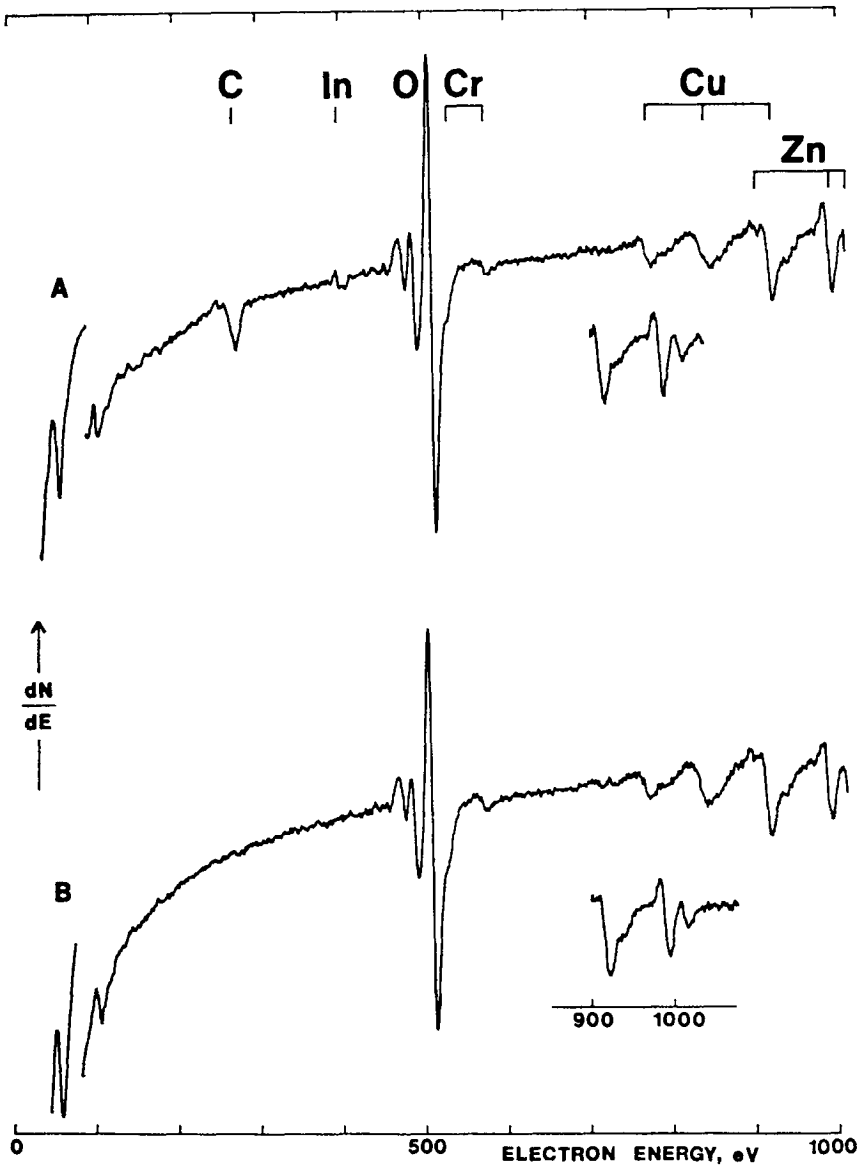

FIG. 5. The Auger spectra of the Cu/Zn/Cr (60:30:10) catalyst (A) after calcination at 350°C and (B) after undergoing testing for methanol synthesis activity. Instrument settings: primary beam-2000 eV at 60 μA; modulation = 5 eV.

or zinc hydroxycarbonates. It is not possible to make assignments on the basis of literature reports of XPS energies of O 1*s* in reference compounds because the published values for the same compound differ by up to 3 eV (*39*, *46*).

Particular attention was paid to tracing carbon during the catalyst preparation and use. Figure 5 shows the Auger spectra of a calcined (A) and used (B) Cu/ZnO/Cr_2O_3 catalyst demonstrating that the carbon peak, be it residual carbonate or an impurity, disappeared and also that carbon deposits were not formed during the use. The displayed surface analysis was typical of all catalyst preparations studied in the present work including catalysts deactivated by reducing the CO_2 concentration in the reaction mixture.

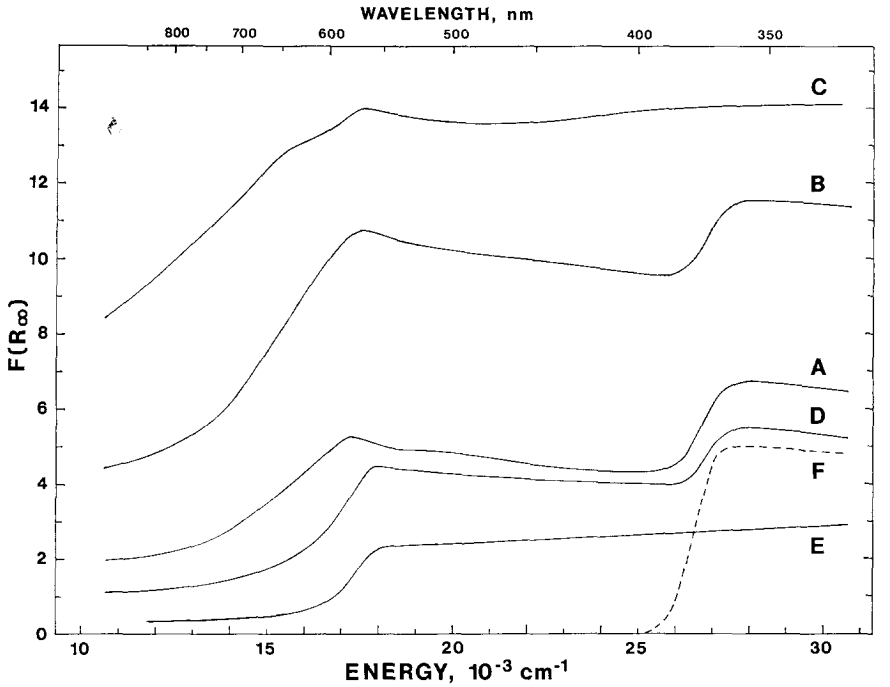

FIG. 6. The diffuse reflectance spectra of reduced Cu/ZnO catalysts that initially contained (A) 5%, (B) 10%, (C) 30%, (D) 67%, and (E) 100% CuO. The dashed line (F) represents the spectrum of pure ZnO. $F(R_\infty)$ is proportional to the absorption coefficient.

Electronic Properties of Catalyst Components and of the Mixed Catalysts

Visual observations of the individual catalyst components and of the low copper-containing mixed catalysts indicated a profound mutual influence of the catalyst components in intimate contact upon each other's electronic spectra. For example, the reduced copper–zinc oxide catalysts were black, despite the presence of only metallic copper (red) and hexagonal zinc oxide (white) phases identified by X-ray diffraction. To characterize the indicated electronic interactions in greater detail, near-infrared–visible-uv absorption spectra of the pure components and of the mixed catalysts were obtained. The electronic absorption spectra of the pure components confirmed the results reported by others, with the characteristic absorption edge of zinc oxide centered at about 373 nm (*41*), the top of the "*d*-hump" of metallic copper near 560 nm (*42*, *43*), the absorption edge of Cu_2O around 610 nm (*44*), and the absorption edge of CuO at approximately 850 nm (*45*).

The spectra of the reduced Cu/ZnO catalysts are displayed in Fig. 6 for the compositions (A) 5, (B) 10, (C) 30, and (D) 67% copper. The spectral features of the pure components are evident in some of the spectra, e.g., the absorption edge of ZnO in curves A, B, and D and the "*d*-hump" of metallic copper in curve D. The latter feature was significantly shifted toward lower energies for the lower copper-containing samples A, B, and C.[1] Visually, the blackness of the reduced catalysts increased in intensity as the copper content increased from 2 to 30%, and this correlates with the main observation derived from Fig. 6; i.e., the intense absorption continuum in the visible and near-infrared

[1] In addition, these specimens exhibited a near-infrared absorption from 600 to 900 nm whose intensity increased with increasing copper content between 5 and 30% Cu. In the spectrum of the 30% Cu sample, a distinct shoulder at 650 nm appeared.

TABLE 3

BET Argon Surface Areas of the Cu/ZnO Catalysts

Catalyst composition CuO/ZnO	Surface area (m^2/g) of	
	Reduced	Used
0/100		25.2
2/98		28.9
10/90		27.0
20/80		30.0
30/70		37.1
40/60		13.5
50/50		10.3
67/33	6.3	8.6
100/0	1.4	—

region increased in intensity as the copper concentration in the sample was increased up to 30%. The continuum and the 650 nm shoulder were also present but less pronounced in the reduced 67% Cu/ZnO catalyst, and this sample exhibited the characteristic red copper color. It is apparent that the near-infrared absorption is present in curve A for the 5% Cu/ZnO sample, and it is of interest to note that ZnO is the only crystallographically identifiable phase in this catalyst. However, prolonged reduction of the 5% Cu/ZnO catalyst led to the appearance of X-ray diffraction lines due to Cu metal with a concomitant reduction of the near-infrared absorption.

Surface Areas and Pore Structures of the Cu/ZnO, Cu/ZnO/Al_2O_3, and Cu/ZnO/Cr_2O_3 Catalysts

The BET surface areas of the Cu/ZnO catalysts are given in Table 3. The surface area of the Cu/ZnO/Al_2O_3 (60/30/10) catalyst tested in the present work was 33.4 m^2/g after use, while the surface area of the Cu/ZnO/Cr_2O_3 (60/30/10) catalyst

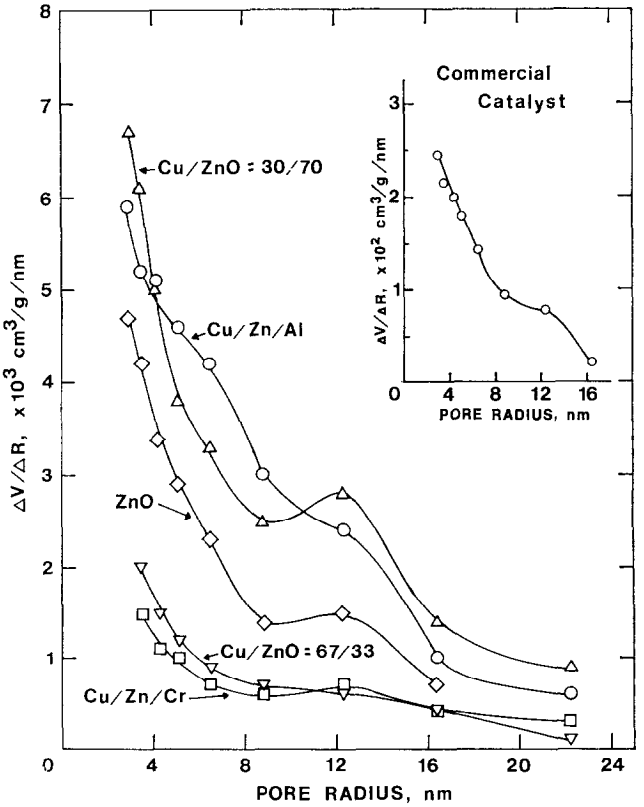

FIG. 7. The mesopore volume distributions (cylindrical pores) for catalysts that had been tested for methanol synthesis activity.

was 15.6 m^2/g after use. The comparable tested $Cu/ZnO/Al_2O_3$ catalyst that had been prepared from the acetates exhibited a final surface area of 26.1 m^2/g. The mesopore distributions of the Cu/ZnO, $Cu/ZnO/Al_2O_3$, and $Cu/ZnO/Cr_2O_3$ catalysts are displayed in Fig. 7 along with the mesopore distribution of a commercial catalyst. The micropore volumes of these catalysts were found to be approximately the following: Cu/ZnO (67/33), 0.3 and 0.6; Cu/ZnO (30/70), 1.0; $Cu/ZnO/Al_2O_3$ (from acetates), 0.0; and $Cu/ZnO/Cr_2O_3$, 1.2 cm^3/g. The commercial catalyst had a micropore volume of about 3.0 cm^3/g at STP.

Catalytic Activities of the Cu/ZnO, $Cu/ZnO/Al_2O_3$, and $Cu/ZnO/Cr_2O_3$ Catalysts in Methanol Synthesis

The catalyst testing was carried out in a flow reactor at a flow rate of 5000 GHSV with a $H_2/CO/CO_2$ = 70/24/6 mixture at 75 atm and in the temperature range of 200 to 300°C. All catalysts investigated here were more than 99% selective to methanol with respect to carbon conversion. Under steady-state conditions, carbon dioxide was not consumed but before steady state was reached, the CO_2 concentration sometimes temporarily decreased with concomitant formation of water.

The activities of the Cu/ZnO catalysts are compiled in Table 4 in terms of carbon conversion and methanol yields per gram of the catalyst as a function of catalyst composition. The table also contains the same activity data per unit total surface area of the catalyst. The activities at 250°C of pure ZnO and pure copper were zero within detection limits that were estimated to be less than 0.005 kg/liter/hr in methanol yield. The activities of the Al_2O_3- and Cr_2O_3-containing catalysts are given in Table 4, and it is evident that they are comparable to the activities of the binary Cu/ZnO catalysts.

Side product analysis showed that no carbon containing products other than methanol were formed over the Cu/ZnO catalysts, approximately 1% of the CO that reacted over the $Cu/ZnO/Al_2O_3$ catalysts formed hydrocarbons, and about 0.8% of the CO reacted over the $Cu/ZnO/Cr_2O_3$ catalysts produced low alcohols, mainly ethanol.

The $Cu/ZnO/Al_2O_3$ (60/30/10) catalyst was also tested in a H_2/CO (76/24) mixture without CO_2. Although this catalyst was again selective to methanol, it was rapidly and irreversibly deactivated from yielding initially 0.95 kg/liter/hr methanol at 250°C to 0.02 kg/liter/hr of methanol at the same temperature after equilibrating in the syngas for 8 hr at ambient temperature prior to testing. This deactivated catalyst was subjected to Auger analysis and no elements other than those normally present in the catalyst surface were found; in particular, the catalyst surface was not contaminated by any detectable amount of carbon. However, examination of this catalyst by optical spectroscopy revealed that the near-infrared absorption disappeared during the catalyst deactivation, and the deactivated catalyst displayed

TABLE 4

The Catalytic Testing Results for the Cu/ZnO Systems Obtained at 250°C, 75 atm, and GHSV = 5000 hr^{-1} with a Syngas of $H_2/CO/CO_2$ = 70/24/6 vol%

Catalyst composition[a] $CuO/ZnO/M_2O_3$	Carbon conversion	Yield (kg/liter/hr)	Yield (kg/kg/hr)	Yield ($kg/m^2/hr$ ($\times 10^5$))
0/100/0	0	0	0	0
2/98/0	0.7	0.02	0.03	0.10
10/90/0	1.0	0.02	0.02	0.70
20/80/0	10.2	0.22	0.24	0.80
30/70/0	51.1	1.10	1.35	3.63
40/60/0	9.6	0.21	0.18	1.33
50/50/0	11.3	0.25	0.20	1.94
67/33/0	21.8	0.48	0.41	4.76
100/0/0	0	0	0	0
60/30/10[b]	40.0	0.95	1.52	5.82
60/30/10[c]	17.0	0.45	0.58	1.73
60/30/10[d]	47.0	1.17	1.01	6.47

[a] Weight percent as the oxides.
[b] M = Al, prepared from the acetates.
[c] M = Al, prepared from the nitrates, tested at 100 atm.
[d] M = Cr, tested at 100 atm.

only the pink color that is characteristic of copper.

DISCUSSION

The activity pattern of the Cu/ZnO system (Table 4) and the comparison of activities of the Cu/ZnO, Cu/ZnO/Al_2O_3, and Cu/ZnO/Cr_2O_3 catalyst (Tables 1 and 2) demonstrate that the active and selective low pressure methanol catalyst requires a simultaneous presence of copper and zinc oxide and that the effects of Al_2O_3 and Cr_2O_3 are secondary. Moreover, optical spectra of active catalysts show continuous absorption in the visible and near-infrared, which disappears upon deactivation of the catalyst in a highly reducing mixture. For this reason, the formation and electronic properties of the black active phase in the mixed catalysts is of prime interest for an explanation of the catalyst function and will be discussed first.

Catalyst Genesis and Electronic Structure

The precipitates in the Cu/Zn system, namely $Cu_2(OH)_3NO_3$(I), $Zn_5(OH)_6(CO_3)_2$ (II), and $(Cu, Zn)_2(OH)_2CO_3$(III), and their relative proportions, did not influence the basic phase composition of the calcined CuO/ZnO or the reduced Cu/ZnO samples; however, they appeared to determine the catalyst dispersion and morphology by mechanisms that can be well understood from the structures of the compounds I, II, and III. It should first be noted that all three precipitates I, II, and III are thermodynamically more stable than simple hydroxides or carbonates of these two metals (*46*). However, hydroxides may well be kinetic precursors of the hydroxy-carbonates or hydroxynitrates as was indeed concluded by Vasserman and Silant'eva from their studies of the precipitation of compound I (*47*). The sequence of reactions based on the Vasserman–Silant'eva mechanism applied to our system is as follows:

$$CO_3^{2-} + H_2O \rightleftarrows HCO_3^- + OH^-, \quad (2)$$

$$Cu^{2+} + 2OH^- \rightarrow Cu(OH)_{2(s)}, \quad (3)$$

$$3Cu(OH)_{2(s)} + Cu^{2+} + 2NO_3^- \rightarrow Cu(NO_3)_2 \cdot 3Cu(OH)_{2(s)}\,(I) \quad (4)$$

$$Zn^{2+} + 2OH^- \rightarrow Zn(OH)_{2(s)}, \quad (5)$$

$$2Zn^{2+} + 4HCO_3^- + 3Zn(OH)_{2(s)} \rightarrow Zn_5(OH)_6(CO_3)_{2(s)}\,(II) + 2H_2O + 2CO_2, \quad (6)$$

$$Zn^{2+} + 2HCO_3^- + Cu(OH)_{2(s)} \rightarrow CuZn(OH)_2CO_{3(s)}\,(III) + H_2O + CO_2. \quad (7)$$

As the precipitation occurred carbon dioxide was in fact released. Reactions (2) through (7) may be used to explain the compositions of the precipitates at various Cu/Zn ratios (Fig. 2). With increasing Cu/Zn ratio, the relative amount of the zinc hydroxycarbonate (II) continuously decreased, indicating an independent precipitation mechanism (Eqs. (5) and (6)). Simultaneously, the amount of the two copper compounds, (I) and (III), increased so that in the range where zinc concentrations are large (Cu/Zn = 0.1 to 0.5) the mixed copper zinc hydroxycarbonate (III) was preferred, whereas at large copper concentrations the copper hydroxynitrate (II) was preferred. Compound III provides for the most intimate mixture of copper and zinc and is known as the mineral rosalite (*48*).

Upon stepwise calcination to 350°C, all three compounds I, II, and III decompose to oxides MO where M is zinc or copper. Compound II gives rise to zinc oxide, compound III to mixed zinc oxide and copper(II) oxide, and compound I to copper(II) oxide. Possibly some copper may be substituted for zinc in compound II and zinc for copper in compound I but the whole precipitation pattern shows a clear preference of zinc for II and copper for I. The structure of the mixed copper zinc hydroxycarbonate III (Fig. 8) is such

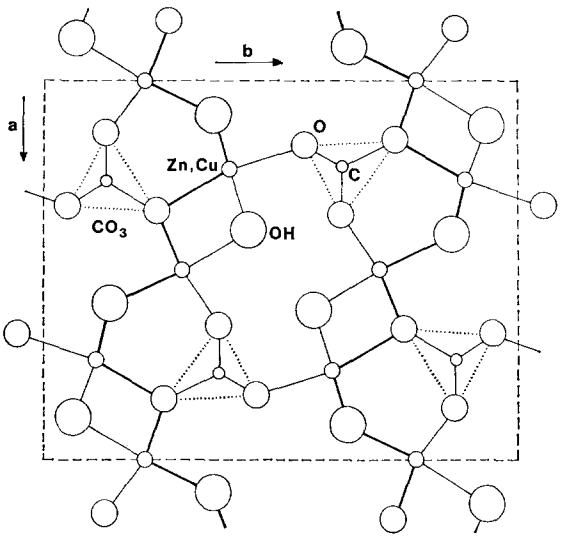

FIG. 8. A representation of the crystal structure of rosalite projected on the (001) plane.

that each metal atom is in square planar or near square planar coordination of oxygen atoms belonging to the OH^- and CO_3^{2-} groups. Its decomposition may be visualized as a condensation of CO_3^{2-} groups with two protons from the nearest OH^- groups which results in the release of $H_2O + CO_2$ along channels parallel to the *c* axis and leaves behind an open network, designated by the heavier lines in Fig. 8, of Cu and Zn atoms square planarly or linearly coordinated to the O atoms originating from the hydroxyl and carbonate groups. This network is structurally related to the tetragonal CuO but not to the hexagonal ZnO. Since ZnO and CuO have to segregate because of their different crystal structures and limited solubilities, the (Cu, Zn) oxide network generated by the decomposition of compound III will initially form a very fine interdispersion of ZnO and CuO with highly imperfect ZnO. On the other hand, at concentrations of 40% copper and higher the ZnO crystallites formed during calcination are well developed into hexagonal platelets (*25*). The platelet morphology coincides with the presence of compound I in the catalyst precursor, indicating that an epitaxial mechanism may be operating in determining the ZnO morphology. Indeed, compound I has pseudohexagonal stable planes (001) of the structure shown in Fig. 9A. That these are surface planes is corroborated by the XPS analysis in which the nitrogen peak corresponding to the hidden nitrate groups is very small compared to those of copper and oxygen. Drawn to scale in Fig. 9B is the triequiangular net of zinc atoms in the basal (0001) plane of ZnO, and Fig. 9C demonstrates that zinc oxide may grow epitaxially on copper hydroxynitrate (I) with its basal plane including the major growth directions. The explanation of hexagonal platelet morphology of ZnO at Cu concentrations equal to or greater than 40% presently proposed is based upon a greater thermodynamic stability of copper hydroxynitrate (I) than that of the carbonates II and III (*46*): As the carbonates II and III decompose during the stepwise calcination, the undecomposed $Cu_2(OH)_3NO_3$ acts as a seed for crystallization of the nascent ZnO which is forced to grow as hexagonal platelets rather than as its normal prismlike habit. Mass spectrometric analyzes of the gases evolved from the copper-rich precursors upon heating indeed showed that the carbonates II

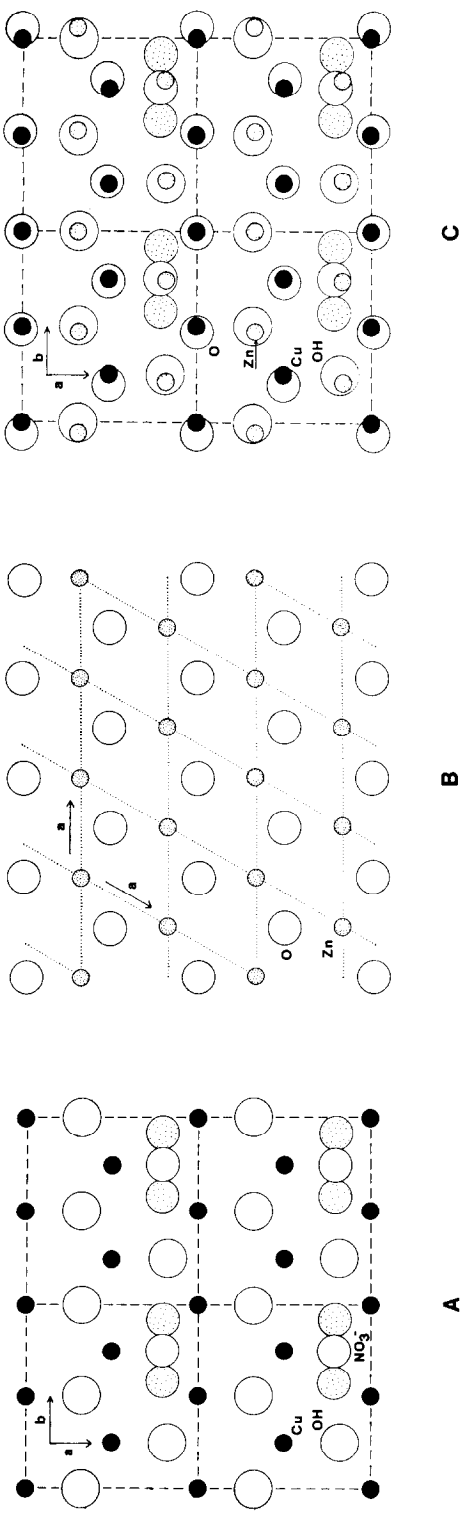

FIG. 9. Representations of (A) the surface structure (001) of $Cu_2(OH)_3NO_3$ that has a layer of exposed copper atoms on which (B) hexagonal ZnO (0001) can easily crystallize (C) along directions in the basal plane.

and III decomposed at a maximum rate at 240°C while the nitrate I at 270°C. In the latter stages of calcination, $Cu_2(OH)_3NO_3$ decomposes into a separate phase of CuO, leaving the ZnO crystallites unchanged. The ZnO morphology is also retained after reduction in which Cu metal is produced from CuO in the mixed samples. Thus, the composition of the precipitates determines the crystal shape and dispersion of ZnO in the final catalyst.

It has already been noted in the Results section that the ZnO crystallites contain, after calcination, 2 to 4% of dissolved CuO at nominal compositions between 15 and 85% CuO. The amount of copper dissolved in ZnO after reduction was even larger, up to 12% in the Cu/ZnO catalysts and up to 16% Cu in the $Cu/ZnO/Al_2O_3$ or Cr_2O_3 catalysts (*25*). At the same time, optical measurements of the binary Cu/ZnO catalysts (Fig. 6) revealed a new strong near-infrared–visible absorption spectrum unlike that of CuO, Cu_2O, Cu metal, or Cu^{II} ions in ZnO (*49*). This new spectrum was most pronounced in the 30/70 Cu/ZnO catalyst in which the ZnO band edge completely disappeared. Thus, although the ZnO possessed its normal crystal structure, its valence-to-conduction band optical transitions were strongly modified by the presence of copper obtained by the reduction of the CuO/ZnO mixed oxide that was not entirely completed to copper metal. The fact that zinc oxide band-to-band transition is influenced provides evidence that the optical changes originate in the zinc oxide lattice and are thus due to solute copper and associated defect structure. The new near-infrared–visible absorption spectrum is assigned to Cu^{I} species dissolved in ZnO. The dissolution of Cu^{I} in ZnO will be favored by the fact that Cu^{I} is isoelectronic with Zn^{II} and that it assumes, like Zn^{II}, a tetrahedral coordination in many of its inorganic compounds. The limitation of Cu^{I} solubility in ZnO consists of the requirement of electroneutrality upon substitution of some Zn^{II} by Cu^{I} which must be ensured either by oxygen vacancies or by interstitial cations. Further increase of Cu^{I} concentration may be obtained if trivalent ions are simultaneously dissolved in ZnO (*25*).

Electronic levels of Cu^{I} in ZnO are expected to be located in the forbidden band of ZnO, as illustrated in Fig. 10. The origin of the band spectrum of ZnO from atomic Zn 4*s*, O 2*p*, and Zn 3*d* levels is shown in Fig. 10A so that the atomic levels, the experimental bandgap of 0.24 Ry (3.2 eV) (*50*), and the theoretical bandwidths of the valence and the Zn 3*d* band (*51*, *52*) are drawn to scale. In comparison to the Zn 3*d* band, which lies *below* the valence band of zinc oxide, the Cu 3*d* band is expected to be located *above* the valence band of the zinc oxide because the Cu 3*d* levels are located well above O 2*p* and are, in fact, as high as the Zn 4*s* levels (Fig. 10B). In addition, the Cu 4*s* level will give rise to band edges similar to the Zn 4*s* level but located higher in the energy scale with the valence band maximum in the bandgap of ZnO. On the basis of the energy levels discussed above, there are two possible sets of new levels of Cu^{I}/ZnO solution: the filled 3*d* band of copper and the sp^3 valence band originating from Cu 4*s* and O 2*p* atomic levels. The transition between the Cu 3*d* band and ZnO conduction band corresponds to charge transfer between the Cu^{I} and Zn^{II} ions which is proposed here to be the principal cause of the intense near-infrared–visible absorption. The degree to which the Cu^{I}/ZnO solution determines the optical and chemical properties of the mixed catalysts depends upon the composition and preparation history: the most intimate mixture of copper and zinc is favored by the precursor III $(Cu, Zn)_2(OH)_2CO_3$ which has a maximum concentration at 30/70 Cu/Zn ratio. This precursor gives rise to a catalyst in which by spectral evidence copper and zinc oxide undergo the most extensive interaction and which is also the most active in methanol

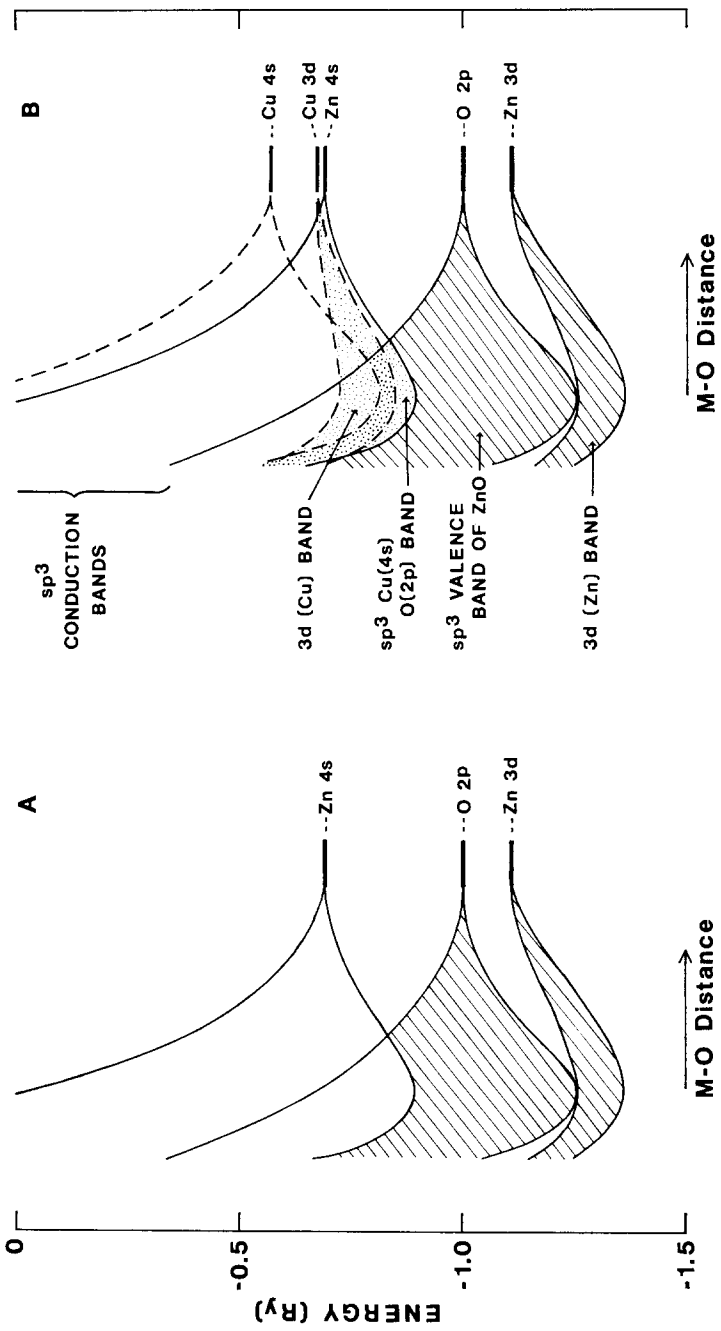

FIG. 10. A diagram showing the band spectra of (A) ZnO and (B) Cu(I)/ZnO solid solution.

synthesis. In addition to the strong absorption by the Cu^I/ZnO solution, the 30/70 Cu/ZnO catalyst also displays the "*d*-hump" absorption at 17,500 cm^{-1} (Fig. 6C) due to metallic copper particles which are in contact with the zinc oxide phase (*25*). The *d*-hump energy in this catalyst is slightly lower than that in free metallic copper (17,900 cm^{-1}) which indicates a small extent of electron transfer from the copper particles into the Cu^I/ZnO solution. As the copper concentration decreases from 30 to 5%, the absorption intensity of the Cu^I/ZnO solution also decreases and the *d*-hump energy is further shifted to lower energies (Fig. 6C, B, and A). In catalysts with high copper concentrations, represented in Fig. 6 by spectrum D for the 67/33 Cu/ZnO composition, the copper *d*-hump energy is exactly that of the free copper metal (Fig. 6E), showing that the copper metal particles in this catalyst have their normal electronic properties independent of the presence of ZnO. However, the absorption due to the Cu^I/ZnO solution is still apparent from the substantially higher intensity of spectrum D of the 67/33 Cu/ZnO catalyst than that of pure copper (spectrum E). The ZnO absorption edge, although weak compared to pure zinc oxide (dashed curve in Fig. 6), is distinctly developed in all except the 30/70 Cu/ZnO catalysts, which demonstrates that the precursor structure plays a unique role in determining the extent of interactions among the components and the activity of the final catalyst. When the mixing of copper and zinc in the precursors is limited, the final catalyst may contain a significant number of ZnO particles with little or no copper dissolved (*25*) and, as a result, will display a lower activity.

A note should be added on the possible role of interstitial zinc and oxygen vacancies in the absorption spectra. Zinc oxide with excess zinc displays a weak absorption in the blue region (*53*) and oxygen vacancies in copper-containing oxides give rise to luminescence and weak absorption in the visible and near-infrared (*44*). Neither of these features alone could account for the near-infrared absorption continuum and its intensity, and thus interstitial zinc and oxygen vacancies may give rise at most to secondary spectral features superimposed on the fundamental band spectrum of the Cu^I/ZnO solution discussed above. A separate experiment confirmed that the reduction and reaction conditions employed in methanol synthesis are not sufficient to produce a visibly detectable color change in pure zinc oxide leaving this compound white after exposure to 2% H_2/98% N_2 at 250°C for 4 hr and to the $H_2/CO/CO_2$ mixture at 75 atm up to 320°C for 10 hr.

Activity Pattern of the Copper–Zinc Oxide-Containing Catalysts and the Synthesis Mechanism

The results of catalytic testing of the Cu/ZnO, $Cu/ZnO/Al_2O_3$, and $Cu/ZnO/Cr_2O_3$ catalysts clearly establish that the Cu/ZnO catalysts have an activity toward methanol synthesis comparable per weight and per unit surface area to those of the $Cu/ZnO/Al_2O_3$ and $Cu/ZnO/Cr_2O_3$ catalysts. Also, the selectivity of the Cu/ZnO catalysts is equal to or exceeds that of the alumina- or chromia-based catalysts. No special pore distribution is necessary for highly effective Cu/ZnO catalysts with or without alumina and chromia, and thus the synthesis appears to proceed as a surface reaction without diffusion control.

The mutual promotion effect of copper and zinc oxide is illustrated by the activity pattern in Table 4, which shows that a substantial activity is displayed by the various intermediate Cu/ZnO compositions while the pure components, i.e., copper metal and zinc oxide, are inactive under the low-pressure regime. From the observations that the activation energy is 30 kcal/mol (*17*) and that comparable activities were obtained for pure ZnO at 350 atm and 400°C (metallic copper had

less catalytic activity than did ZnO) and Cu/ZnO at 75 atm and 250°C, it is estimated that the catalytic activity of the binary catalyst is at least three orders of magnitude greater than those of the pure components. Since no new phase other than the normal crystal structures of Cu metal and zinc oxide exists in the mixed Cu/ZnO catalysts, the promotion effect can only stem from the catalytic activity of a solid solution such as the Cu^{I}/ZnO system described in the previous paragraph, from uncommon crystal planes and surface imperfections stabilized by the presence of the second phase, and from long range effects resulting from electron transfer between the active and support phases. Only the dominant effect that is associated with the new electronic structure of the Cu^{I}/ZnO solution will be discussed here, and the effects of crystal morphology are reported in detail elsewhere (*25*). It should only be noted that both principal ZnO morphologies, the rodlike network bounded by prism planes predominant at 2–30% Cu/ZnO and the hexagonal platelets bounded by the basal plane occurring at 40–67% Cu/ZnO, are catalytically active and selective to methanol. The rodlike networks have a higher surface area and, hence, a higher activity than the platelets, provided that enough Cu^{I} is dissolved in the zinc oxide. Considerations of long-range electron transfer in small crystallites in contact with supporting phase, although conceptually developed (*54*), give rise to estimates of only marginal effects on the surface equilibria in the present system.

The mechanism of the catalytic function of the Cu^{I}/ZnO solution proposed here is based on the known properties of zinc oxide and univalent copper. Zinc oxide is a good hydrogenation catalyst (*55*) that activates hydrogen by heteropolar splitting giving rise to ZnH and OH groups on the ZnO surface (*56*). However, the chemisorption activity of ZnO toward CO is poor (*57*, *58*), evidently because of unavailability of the deeply lying Zn 3*d* orbitals for backdonation. The behavior of Cu^{I} in various low coordinated compounds and surfaces is just the opposite: certain Cu^{I} compounds quantitatively absorb carbon monoxide in solutions (*59*) and Cu^{I} ions in zeolites form 1:1 complexes with carbon monoxide (*60*) while they do not absorb hydrogen up to 100 to 150°C (*61*). The binding of CO by Cu^{I} can be easily understood from the high energy and spatial extent of the unscreened Cu 3*d* orbitals available for backbonding into the π^* orbitals of CO.[2] Similar CO bonding is proposed here for the Cu^{I} centers in ZnO: the Cu 3*d* orbitals are now broadened into a band as indicated in Fig. 10, but they are still the highest occupied orbitals suited for backbonding into the π^* orbitals of CO.

The initial step of methanol synthesis over the Cu/ZnO catalyst is thus proposed to be chemisorption and activation of CO on the Cu^{I} centers and of hydrogen on the surrounding ZnO surface. The hydrogenation of CO may proceed in a series of subsequents steps, one of which must effect hydrogenation of the oxygen end of CO and another the hydrogenolysis of the Cu–C bond. A possible complete mechanism involving formyl (iii) and hydroxycarbene (iv) intermediates is illustrated below.

[2] The energy of the 3σ orbital of CO is given by its ionization potential, −14.0 eV (cf. H. D. Hagstrum and J. T. Tate, *Phys. Rev.* **59**, 354 (1941)), and that of the π^* orbital is −5.94 eV, as determined from the $A^1\pi$ state excitation energy (cf. G. Herzberg, "Molecular Spectra and Molecular Structure," Vol. I, 2nd ed., p. 452, Van Nostrand, Princeton, N.J., 1950). Thus the direct donation from CO (3σ) orbitals into the Cu^{I}/ZnO lowest-lying empty band with band edge lying above the Fermi level of ZnO, −4.4 eV, has a low probability and hence a small contribution to bonding. On the other hand, the full Cu^{I}(3*d*) levels located in the ZnO bandgap between −6 eV and −3 eV have energies equal to or greater than that of the empty CO(π^*) orbital and are thus very well suited for backdonation.

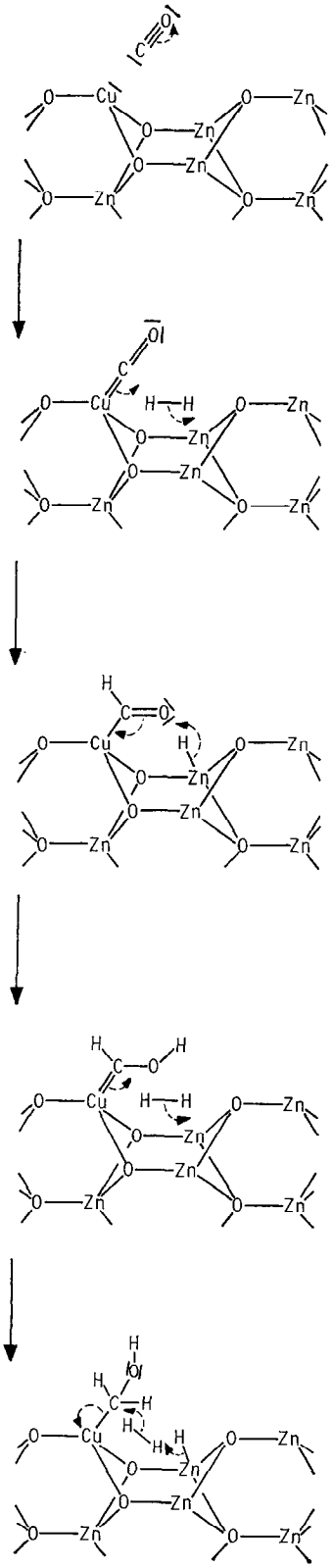

(i) (ii) (iii) (iv) (v)

The mechanism is represented here for the prism plane of ZnO but other surface planes including the basal planes of ZnO can promote the same set of reactions. The heteropolar splitting of hydrogen and the binding of CO to cationic Cu^{I} centers represents an electrophilic attack of the carbon end of CO by protons and a nucleophilic attack on the oxygen end of CO by hydride ions, if the complex process involving the electron equilibria in the semiconductor surface can be expressed in the simplified language of the mechanistic chemistry of organic molecules. The hydrogenolysis of the $Cu–CH_2OH$ bond is proposed to be a limiting step in view of earlier reports that a CH_3O composition persisted on the catalyst surface when exposed to H_2:CO mixtures ranging from 1:20 to 100:1 (*62*).

Effects of Poisons and Oxidizing Gases on the Synthesis

The sensitivity of copper-containing methanol synthesis catalysts to poisoning by sulfur has been known for a long time, and, in fact, Natta rejected the copper-containing catalysts as impractical because of their rapid deactivation in the presence of hydrogen sulfide (*17*). He attributed the sulfur poisoning to the formation of bulk CuS according to reaction (8):

$$Cu + H_2S = CuS + H_2, \quad K_{550°K} = 3.2. \quad (8)$$

Another bulk sulfide might be formed by reaction (9):

$$2Cu + H_2S = Cu_2S + H_2, \qquad K_{550°K} = 3.32 \times 10^4. \quad (9)$$

However, it was found that the copper-containing catalysts were poisoned by levels of H_2S as low as 0.1 ppm (*14, 17, 35*), an effect that cannot be accounted for either by reaction (8) or by (9). Reaction (8), because of its small equilibrium constant, does not come into consideration for sulfide formation until the H_2S

concentration in hydrogen reaches 24%, and reaction (9) has equilibrium shifted to the right only at more than 30 ppm of H_2S, while the catalysts are severely poisoned at substantially lower levels.

According to the presently proposed synthesis mechanism, the active catalyst is a zinc oxide phase with dissolved Cu^I species, and a simple surface poisoning reaction may be suggested in which no hydrogen is produced and therefore a substantially greater driving force than in reactions (8) and (9) exists for the formation of the right-hand side products of reaction (10):

$$Cu^I + O^{2-} + H_2S = Cu^ISH^- + OH^-. \quad (10)$$

Similarly, halogen poisoning, e.g., by hydrogen chloride (*16*), may initially proceed as a surface reaction giving rise to Cu^ICl^- and OH^- species, followed by escape of the rather volatile copper(I) chloride into the gas phase and an irreversible removal of the Cu^I centers from the catalyst.

In contrast to the poisoning by sulfur and halogen containing gases, methanol yields are enhanced by the presence of carbon dioxide, water, and oxygen. Both oxygen and water increased the yields more than an equivalent amount of carbon dioxide (*12*), and preliminary experiments in the present investigation utilizing pulsed additions of oxygen to the CO/H_2 feed gas indicated that up to a 15-fold increase of methanol yields could be obtained (*63*). An additional observation of interest was made in the present work: in the absence of CO_2 (or H_2O and O_2), the catalyst gradually lost activity with concomitant change of color from black to pink with no carbon deposition and very little change in surface area. The physical changes accompanying the catalyst deactivation indicated that the active Cu^I/ZnO phase was reduced to inactive copper metal by the reaction mixture CO/H_2. In view of this mechanism of deactivation, the rate-enhancing effect of oxygen, water, and carbon dioxide is to decrease the reduction potential of the CO/H_2 feed gas and to keep Cu^I in the active Cu^I/ZnO state. It should be noted that the virtual oxygen pressures for the CO_2/CO and H_2O/H_2 ratios frequently employed in the synthesis are sufficient for preventing the reduction of Cu^I to fine copper dispersions but not to bulk copper metal so that the reduction deactivation mechanism is irreversible once large crystallites of copper metal are produced from the Cu^I/ZnO phase.[3] The principal role of CO_2 (and also of water and oxygen) thus appears to be to maintain the catalyst in an active state rather than to undergo a direct hydrogenation to methanol. Such a role is consistent both with the presently proposed reaction mechanism and with the lack of CO_2 consumption under a steady state operation of the synthesis. Since the catalyst surfaces were found to be carbon-free under a variety of reaction conditions, carbon removal by CO_2 does not contribute to the promotion effects of carbon dioxide.

ACKNOWLEDGMENTS

The authors express their gratitude to Professor W. Keith Hall for suggesting to them research on methanol synthesis catalysts and for his constant interest in this work. Support for this research was provided by the Electric Power Research Institute (RP779-12), the Energy Research and Development Administration, and the National Science Foundation (AER-7503776).

REFERENCES

1. Bröcker, F. J., Marosi, L., Schröder, W., and Schwarzmann, M., German Patent 2,056,612 (May 31, 1972); assigned to Badische Anilin- & Soda-Fabrick AG.

[3] Virtual oxygen pressures at 275°C for $CO_2/CO = 6/24$ and $H_2O/H_2 = 1/100$ are 9×10^{-46} and 2.5×10^{-46} atm, respectively. The oxygen pressure for oxidation of bulk Cu metal to Cu_2O is 4.4×10^{-25} atm and for oxidation of copper atoms to Cu_2O is less than 10^{-99} atm. The Cu^I/ZnO solution is, up to the solubility limit, thermodynamically more stable than Cu_2O, and should be therefore even less reducible in the above CO_2/CO and H_2O/H_2 mixtures.

2. Catalysts and Chemicals, Inc., German Patent 1,965,007 (Oct. 15, 1970).

3. Collins, B. M., German Patent 2,302,658 (Aug. 2, 1973); assigned to Imperial Chemical Industries, Ltd.

4. Shishkov, D. S., and Kasabova, N. A., *Dokl. Bulg. Akad. Nauk.* **27**, 73 (1974).

5. Imperial Chemical Industries, Ltd., French Patent 1,489,682 (July 21, 1967).

6. Imperial Chemical Industries, Ltd., French Patent 2,037,567 (Dec. 21, 1970).

7. Kotera, Y., Oba, M., Ogawa, K., Shimomura, K., and Uchida, H., *in* "Preparation of Catalysts" (B. Delmon, P. A. Jacobs, and G. Poncelet, Eds.), pp. 489–597. Elsevier, Amsterdam, 1976.

8. Stiles, A. B., German Patent 2,320,192 (Oct. 25, 1973); assigned to E. I. du Pont de Nemours and Co.

9. Lender, Yu. V., Tsybina, E. N., Popov, I. G., Pirozhenko, L. F., and Petrishcheva, G. S., *Khim. Prom. (Moscow)* **49**, 899 (1973).

10. Oliver, R. B., German Patent 1,229,990 (Dec. 8, 1966); assigned to Power-Gas Corp., Ltd.

11. Eguchi, T., Yamamoto, T., Yamauchi, S., Kuraishi, M., and Asakawa, K., U.S. Patent 3,256,208 (June 14, 1966); assigned to Japan Gas-Chemical Co., Inc.

12. Bröcker, F. J., German Patent 2,116,949 (Oct. 19, 1972); assigned to Badische Anilin- & Soda-Fabrik AG.

13. Jorgensen, M. H., and Rüshede, K., German Patent 2,016,596 (Dec. 3, 1970); assigned to Topsoe, Haldor Frederik Axel.

14. Davies, P., and Snowdon, F. F., U.S. Patent 3,326,956 (June 20, 1967); assigned to Imperial Chemical Industries, Ltd.

15. Baron, G., Bechtholdt, H., Bratzler, K., Leibgolt, H., and Ehrland, E., German Patent 1,300,917 (Aug. 14, 1969); assigned to Metallgesellschaft AG.

16. Dewing, J., and Davis, D. S., *Adv. Catal.* **24**, 221 (1975).

17. Natta, G., *in* "Catalysis" (P. H. Emmett, Ed.), Vol. III, pp. 349–411. Reinhold, New York, 1955.

18. Leonov, V. E., Karabaev, M. M., Tsybina, E. N., and Petrishcheva, G. S., *Kinet. Katal.* **14**, 970 (1973); English translation, p. 848.

19. Kagan, Yu. B., Lin, G. I., Rozovskii, A. Ya., Loktev, S. M., Slivinskii, E. V., Bashkirov, A. N., Naumov, I. P., Khludenev, I. K., Kudinov, S. A., and Golovkin, Yu. I., *Kinet. Katal.* **17**, 440 (1976); English translation, p. 380.

20. Rozovskii, A. Ya., Lin, G. I., Liberov, L. G., Slivinskii, E. V., Loktev, S. M., Kagan, Yu. B., and Bashkirov, A. N., *Kinet. Katal.* **18**, 691 (1977); English translation, p. 578.

21. Kagan, Yu. B., Rozovskii, A. Ya., Lin, G. I., Slivinskii, E. V., Loktev, S. M., Liberov, L. G., and Bashkirov, A. N., *Kinet. Katal.* **16**, 809 (1975).

22. Rozovskii, A. Ya., Kagan, Yu. B., Lin, G. I., Slivinskii, E. V., Loktev, S. M., Liberov, L. G., and Bashkirov, A. N., *Kinet. Katal.* **16**, 810 (1975).

23. Poutsma, M. L., Elek, L. F., Ibarbia, P. A., Risch, A. P., and Rabo, J. A., *J. Catal.* **52**, 157 (1978).

24. Shimomura, K., Ogawa, K., Oba, M., and Kotera, Y., *J. Catal.* **52**, 191 (1978).

25. Mehta, S., Simmons, G. W., Klier, K., and Herman, R. G., *J. Catal.*, in press.

26. Tunell, G., Posnjak, E., and Ksanda, C. J., *Z. Kristallogr.* **A90**, 120 (1935).

27. Bunn, C. W., *Proc. Phys. Soc. London* **47**, 835 (1935).

28. Joint Committee on Powder Diffraction Standards, "Powder Diffraction File Search Manual—Inorganic (Fink Method)," Swarthmore, Pa., 1973.

29. "International Tables for X-ray Crystallography," (K. Lonsdale *et al.*, Eds.), Vol. 3. Kynock Press, Birmingham, England, 1954.

30. Cullity, B. D., "Elements of X-ray Diffraction." Addison-Wesley, Reading, Mass., 1956.

31. Klier, K., *Catal. Rev.* **1**, 207 (1967).

32. Brunauer, S., Mikhoil, R. Sh., and Bodor, E. E., *J. Colloid Interface Sci.* **24**, 451 (1967).

33. Bodor, E. E., Odler, I., and Skalny, J., *J. Colloid Interface Sci.* **32**, 367 (1970).

34. Sing, K. S. W., Surface area determination, *in* "IUPAC Symp. Proceedings, Bristol, U. K., 1969."

35. Nowacki, W., and Scheideggar, R., *Helv. Chim. Acta* **35**, 375 (1952).

36. Ghose, S., *Acta Crystallogr.* **17**, 1051 (1964).

37. Wells, A. F., *Acta Crystallogr.* **4**, 200 (1951).

38. Cornthwaite, D., British Patent 1,296,212 (Nov. 15, 1972); assigned to Imperial Chemical Industries, Ltd.

39. McIntyre, N. S., and Cook, M. G., *Anal. Chem.* **47**, 2208 (1975).

40. Frost, D. C., Ishitani, A., and McDowell, C. A., *Mol. Phys.* **24**, 861 (1972).

41. Scharowsky, E., *Z. Phys.* **135**, 318 (1953).

42. Roberts, S., *Phys. Rev.* **118**, 1509 (1960).

43. Beaglehole, D., *Proc. Phys. Soc. London* **85**, 1007 (1965).

44. Bloem, J., *Phillips Res. Rept.* **13**, 167 (1958).

45. Stone, F. S., *Bull. Soc. Chim. Fr.* **1966**, 819 (1966).

46. Rossini, F. D., Wagman, D. D., Evans, W. H., Levine, S., and Jaffe, I., "Selected Values of Chemical Thermodynamic Properties," National Bureau of Standards Circular No. 500, 1952.

47. Vasserman, I. M., and Silant'eva, N. I., *Russ. J. Inorg. Chem.* **13**, 1041 (1968).

48. Donnay, S. D. H., and Ondik, H. M., "Crystal Data: Determinative Tables," Vol. 2. National Bureau of Standards, Washington, D.C., 1973.

49. Weakliem, H. A., *J. Chem. Phys.* **36**, 2117 (1962).

50. Klucker, R., Nelkowski, H., Park, Y. S., Skibowski, M., and Wagner, T. S., *Phys. Stat. Sol.* (*b*) **45**, 265 (1971).

51. Rössler, V., *Phys. Rev.* **184**, 733 (1969).

52. Bloom, S., and Ortenburger, I., *Phys. Stat. Sol.* (*b*) **58**, 561 (1973).

53. Heiland, G., Mollwo, E., and Stöckmann, F., *Solid State Phys.* **8**, 191 (1959).

54. Klier, K., *Collect. Czech. Chem. Commun.* **27**, 920 (1962).

55. Kokes, R. J., and Dent, A. L., *Adv. Catal.* **22**, 1 (1972).

56. Eischens, R. P., Pliskin, W. A., and Low, M. J. D., *J. Catal.* **1**, 180 (1962).

57. Cimino, A., Molinari, E., and Cipollini, E., *in* "Proceedings 2nd Internat. Congr. Catalysis, 1960," p. 263.

58. Hart, P. M. G., and Sebba, F., *Trans. Faraday Soc.* **56**, 551 (1960).

59. Cotton, F. A., and Wilkinson, G., "Advanced Inorganic Chemistry," 2nd ed., p. 898. Interscience, London, 1966.

60. Huang, Y. Y., *J. Catal.* **30**, 187 (1973).

61. Texter, J., Strome, D. H., Herman, R. G., and Klier, K., *J. Phys. Chem.* **81**, 333 (1977).

62. Tsuchiya, S., and Shiba, T., *Bull. Chem. Soc. Japan* **38**, 1726 (1965).

63. Klier, K., "Advanced Methanol Synthesis Catalysts," Second Semi-Annual Technical Progress Report to ERDA and NSF (RANN), Grant No. AER-75-03776, December 10, 1976.